JOURNAL OF THERMOPHYSICS AND HEAT TRANSFER
Vol. 17, No. 2, April–June 2003

# Testing and Modeling Thermosyphonic Closed-Loop Magnetohydrodynamic Electrolyte Flow

Nesreen Ghaddar* and Elie Sawaya†
*American University of Beirut, Beirut 1107 2020, Lebanon*

**An experimental and analytical study is presented of thermosyphonic magnetohydrodynamic (MHD) flow of electrolyte solutions using permanent magnets to produce the magnetic field. For this purpose, a thermosyphonic closed loop MHD flow system is built and tested. The heated upper and cooled lower parts of the loop are constructed from copper pipe coated with varnish on the inside surface. The middle region is made from Plexiglas® vertical pipes, with copper electrodes placed opposite to each other on the inside, and a transverse magnetic field applied by a set of permanent magnets. Measurements of the induced flow rate and open circuit voltage are reported as a function of driving temperature difference and magnetic field strength. An analytical one-dimensional model of the flow is used to predict the output voltage and flow bulk velocity. The model is extended to account for the electrode design and the Hall effect pertinent to electrolyte solutions. The developed model has captured the important physical and electrical characteristics of the flow and compares well with experimental data. The work has resulted in evaluating the Hall parameter ($\omega\tau$) of electrolytic solutions, as a function of temperature and electrical conductivity of the fluid. It is found that ($\omega\tau$) can be as large as 100 for electrolytes and causes a significant loss in power output at the electrodes.**

## Nomenclature

$B_0$ = magnetic field strength, T
$C$ = specific heat
$D$ = loop pipe diameter
$D_e$ = spacing between the electrodes
$E_{oc}$ = open-circuit electric field, V/m
$f$ = friction factor for laminar pipe flow
$Gr$ = Grashof number, $g\beta\Delta\ TD^3/\nu^2$
$g$ = gravitational acceleration
$Ha$ = Hartmann number, $B_0 D(\sigma/\rho_0\nu)^{1/2}$
$h$ = heat transfer coefficient in the loop channel
$I$ = electric current, A
$J_y$ = induced electric current density
$L$ = vertical height of the loop
$l$ = height of the insulated region
$m$ = $4h/(\rho C V_0) = Nu/Re_D Pr$
$Nu$ = Nusselt number, $hd/k$
$Pr$ = Prandtl Number, $\nu/\alpha$
$p$ = pressure
$Re$ = Reynolds number, $V_0 D/\nu$
$T$ = temperature
$V_{oc}$ = open-circuit voltage, V
$V_0$ = bulk-induced velocity in the loop
$x, y$ = Cartesian coordinates
$\alpha$ = thermal diffusivity
$\beta$ = thermal expansion coefficient
$\Delta T$ = temperature difference between hot and cold parts
$\theta$ = dimensionless temperature, $(T - T_c)/(T_H - T_C)$
$\mu$ = fluid viscosity
$\nu$ = kinematic viscosity of the fluid
$\rho_0$ = density of the fluid
$\sigma$ = electrical conductivity
$\tau_s$ = shear stress in the channel
$\omega\tau$ = Hall parameter

*Subscripts*

$b$ = bulk values
$C$ = cold
$H$ = hot

## Introduction

THERMOSYPHONIC motion in closed loops plays an important role in the design of thermal energy systems, which are characterized by at least one heat source and some heat sink positioned at some height above the source. When a transverse magnetic field is applied on an electrically conducting fluid in the loop, convective motion is damped, and an electric current is induced. The induced electric current is significant when liquid metal solutions are used, but is very small for electrolyte solutions. Electrolytes have a low electrical conductivity and a high Hall parameter value that warrant their use for magnetohydrodynamic (MHD) power generation. In general, electrical conductivity is a property that represents the ease with which an electrical charge can be transported through a conductor. In a solid conductor such as copper, the charge transport is confined to one dimension. In gases, an electron with a charge has a random thermal motion, which causes it to collide with the atoms, molecules, and ions of the gas with a mean free time $\tau$ between collisions. This time is a function of the density of the particle, the momentum transfer cross section, and the mean random velocity of electrons. The other important quantity in gaseous conductors is the frequency of their circular orbit, which an electron describes in a magnetic field. This quantity is called the cyclotron frequency $\omega$ and its value in radians per second is proportional to the magnetic field strength. In a gaseous conductor, both the electrons and positive ions can move under the action of electromagnetic forces. The diffusion velocity of ions may not be negligible compared to that of electrons, causing what is called the ion slip, and charged particles in a magnetic field tend to move in a direction perpendicular to both the magnetic and induced electric fields. This is the well-known Hall current in the direction of the fluid motion (see Ref. 1). The

Received 2 January 2002; revision received 15 August 2002; accepted for publication 13 September 2002. 

*Professor, Mechanical Engineering Department, Faculty of Engineering and Architecture, P.O.Box 11-236, Riad El Solh; farah@aub.edu.lb. Senior Member AIAA.

†Graduate Student, Mechanical Engineering Department, Faculty of Engineering and Architecture, P.O.Box 11-236, Riad El Solh.

Hall current is negligible when the product of $\omega\tau$, known as the Hall parameter for the ionized gas, is much smaller than unity ($\omega\tau \ll 1$). The Hall parameter is proportional to the magnetic field and is a function of density and temperature of the ionized gas (see Refs. 2 and 3). In electrolytes, a similar effect takes place when the moving fluid is subjected to electromagnetic forces. This effect results from the influence of the magnetic field on the induced current itself in the moving fluid where ions are not confined, leading to an alternative generation concept.[2]

The interest in MHD electrolyte flow is revived in energy systems that require control of flow destabilization or damping of motion where applications extend to reducing drag on objects moving in seawater. Weier et al.[3] presented an overview of experimental results of boundary-layer control by means of electromagnetic forces. Their investigation focused on the use of wall parallel Lorentz forces in the streamwise direction to control a flat plate boundary layer and flow separation on hydrofoils. Furthermore, Weier et al. worked on cylinder wake stabilization in an electrolyte solution by means of electromagnetic forces localized on the cylinder surface.[4]

Hydrodynamic and thermal aspects of convective motion characteristics of single-phase closed-loop thermosyphon have been much discussed in literature. Creveling et al.[5] studied the dynamics of the thermosyphonic flow in single circular loop system exhibiting typical nonlinear effects using one-dimensional analysis and verified their model with experimental observations. Recently, Erhard et al.[6] and Erhard and Muelleur[7] derived a one-dimensional model based on realistic heat transfer law for natural convection in a closed loop and performed experiments to validate the model predictions for symmetric and nonsymmetric arrangement of heat sources and sinks. In previous work, laminar thermosyphonic steady flow in closed-plane channel loop in a transverse magnetic field was studied by Ghaddar[8] using a one-dimensional analytical model and by Ghaddar[9] using a two-dimensional spectral element numerical model. The relevant analytical model predicted values of induced flow velocity and induced current, which compared favorably with the numerical model.[8] However, the model did not take into account the electrode design and the type of electric output connection.

No previous experimental investigation has been reported on thermosyphonic MHD flow of electrolytes. In this work, it is intended to test experimentally the thermosyphonic MHD flow using sodium chloride solution as the circulating fluid in a cylindrical channel. A functional relationship is developed between the induced electric current and the magnetic field strength under different driving thermal conditions for a loop with circular cross section. The one-dimensional model is modified for the special conditions of the system, where only a portion of the loop is exposed to a transverse magnetic field. The developed model will take into account the electrode design and the Hall parameter. Experimental measurements will be compared with the model predictions.

## Experimental Apparatus

### Closed-Loop Setup

The vertical thermosyphonic closed-loop setup is shown in Fig. 1. It consists of a tubular closed loop. The upper and lower parts of the loop are constructed from copper pipes coated with varnish on the inside to yield electrically nonconducting walls. The middle region connecting the upper and lower parts of the loop is made from vertical plexiglass pipes. The working fluids are mainly NaCl and KCl solutions. A filling top tube and a valve serve as vent for the loop and a bottom outlet that serves as a drain. The lower part of the loop (copper tubes) is immersed in a hot water stainless steel reservoir, insulated with a 50-mm fiberglass layer. The reservoir is electrically heated and controlled with an Ultraterm heating unit with proportional integral derivative (PID) control and can withstand temperatures of up to 100°C. The dimensions of the bath are $170 \times 550 \times 330$ mm. The Ultraterm unit provides tight control over temperatures. The upper part of the loop is enclosed in a cooling cylinder of $150 \times 250$ mm in which cooling water is circulated from the cooling unit, where the temperature is also PID controlled. The transverse magnetic field is imposed using permanent magnets that

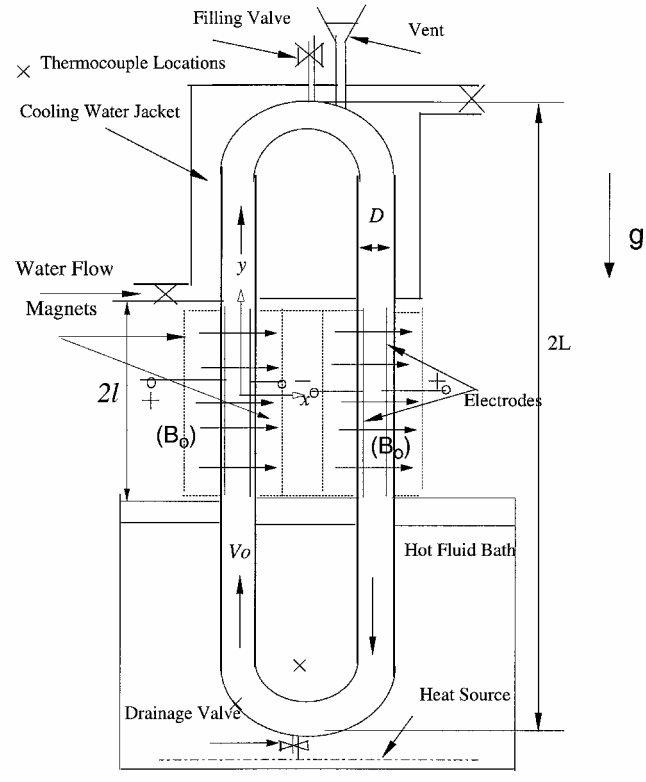


**Fig. 1 Vertical thermosyphonic closed-loop setup.**

are capable of providing a magnetic field of 0.225 T in the fluid. The permanent magnets are placed opposed to each other perpendicular to the electrodes in the middle region of the loop (100 mm long) between the heated reservoir and the cooling compartment using a stand made of aluminum. The two types of magnets used are the sintered neodymium iron boron type of dimensions $100 \times 50 \times 6$ mm (NIBL00127 and NIBL00561) and the sintered ferrite of dimensions $100 \times 100 \times 5$ mm (SFBL00210 and SFBL00211). When only the neodymium iron magnets are used, a magnetic field of 0.1 T was obtained. Using both magnets of ferrite and neodymium added together to created a magnetic field of 0.225 T. The strength of the magnetic field is calculated[10] and measured using an F.W. Bell hand-held Gauss meter Model 4048, with a range of up to 2 T, resolution of 0.01 mT, and accuracy of ±2% in the various settings of the experiment in presence of the liquid at 20°C. The change in the magnetic field strength was less than 2.5% with temperature change from 20 to 80°C.

Electrodes are placed in the middle insulated region opposite to each other on the inner plastic tube wall. The connection of the electrodes to the data acquisition system is performed by heat resistances and isolated copper wires pinched and welded to the electrodes. Three different electrode designs are used in the experiments representing combinations of the electrode type and its electric connection for output: 1) segmented electrode with Faraday generator connection, 2) continuous electrodes with Faraday generator connection, and 3) segmented electrode with Hall generator connection. The continuous electrodes are made of continuous copper sheets cut to required dimensions, where a copper wire is pinched and welded. The electrodes are placed inside the tube and fixed to the surface using transparent epoxy glue. For the segmented electrodes type, two integrated electrode boards are mounted into the straight insulated region, opposing each other and perpendicular to the magnetic field. Each board measures 8 mm in width, 80 mm in length, and 1 mm in thickness. A slot is machined into the Plexiglas tube to fit the electrode board in it. The board laminate is made from epoxy resin FR-4, a material commonly used for printed circuit boards. The top of each board features the 20 electrodes, and wires are connected from the bottom to the electrodes and welded. The electrode segments are 2 mm wide and extend across the entire width of the

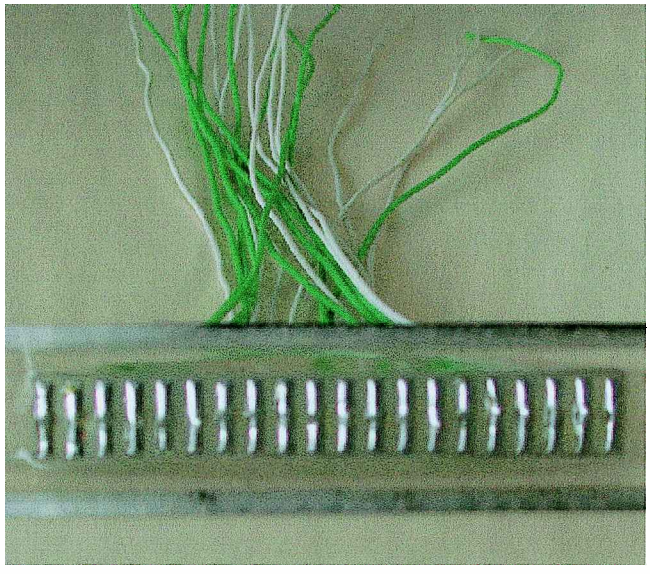

**Fig. 2 Segmented electrode board design.**

board, and subsequent electrodes are spaced 4 mm apart (center to center) as shown in Fig. 2. The different experimental modules based on electrode design, electrode connection, loop geometry, and conditions are summarized as follows:

Module 1 is a segmented electrodes module, connected as a Hall generator (case 3). The specifications of this model were $L = 220$ mm, $l = 60$ mm, $D = 20$ mm, and $w = 100$ mm. The total electrode dimensions are length = 30 mm and width = 25 mm.

Module 2 is a round continuous electrodes model, connected as Faraday generator (case 2). The specifications of this model were $L = 170$ mm, $l = 50$ mm, $D = 20$ mm, and $w = 100$ mm. The electrode dimensions are length = 80 mm and width = 25 mm. Two pairs of electrodes are used, one pair for each side of the loop.

Module 3 has square continuous electrodes and Faraday generator connection (case 2). The electrodes in this module are flat and parallel to each other in a direction perpendicular to the magnetic field. The specification of this model were $L = 212.5$ mm, $l = 62.5$ mm, $D = 24.3$ mm, and $w = 100$ mm. Distance between the electrodes $D_e = 22$ mm. The electrodes' dimensions were length = 120 mm and width = 22 mm. The insulated region is made in a rectangular box shape with dimensions of $30 \times 35 \times 125$ mm.

Module 4 is a segmented electrodes model, with Faraday generator connection (case 1). The specifications of this model are $L = 200$ mm, $l = 50$ mm, $D = 20$ mm, and $w = 100$ mm. The electrode overall dimensions were length = 80 mm and width = 8 mm.

All dimensions and distances are measured with a digital vernier caliper accurate to within $\pm 0.003$ mm.

#### Testing Facility and Instrumentation

The experimental apparatus and instrumentation of the MHD thermosyphonic loop testing facility consisted of the following: Horiba conductivity meter, with a range of 200 mS/cm, resolution of 0.1 mS/cm, and accuracy of $\pm 1\%$; a Fluke 52 K/J digital thermometer used with a K-type thermocouple, measurement range from $-200$ to $+1370$°C, with a resolution of 0.1°C, and accuracy of $\pm 0.1\%$ of reading $+0.7$°C; two Tektronics multimeters; one Hewlett Packard (HP) 6-digits multimeter with a precision error of $\pm .001$ mV; and a Julabo refrigerated circulator with pressure pump of 20 l/min flow and suction pump of 14 l/min flow with valves to control the flow. Temperature was PID controlled with a stability of $\pm 0.01$°C and a range from $-33$ to 200°C. It had a filling volume of 12–16 liters. The Ultraterm heating unit could heat up to 200°C and has $\pm 0.1$°C temperature stability. It was equipped with an internal circulation pump of 12 l/min. A computerized data acquisition system was used for the measurements of model 4 because of the high number of electrode pairs. The computerized data acquisition system consisted of a personal computer with Pentium III processor, one National Instruments SCXI 1000 chassis, 2 National Instruments SCXI 1100 multiplexers that can take 32 differential channels each and can read 2 samples/s with a 4-Hz low-pass filter, 2 National Instruments SCXI 1300 terminal blocks with temperature compensation units, a National Instruments data acquisition board AT-MIO-16E with 8 analog input channels, connecting shielded cables and LAB View software to operate the hardware.

#### Experimental Procedure

The working fluid of the loop is prepared with tap water heated to 25°C. Salt was added until the reading from the conductivity meter indicated the required conductivity (15 or 20 S/m). The conductivity meter maximum scale reading was 20 S/m. The loop is then filled with the working fluid. Before immersing the loop in the hot bath and while the upper cylinder is still empty, voltage readings are taken to check for any bias, to be removed from the readings at the end of the experiment. Then, a Plexiglas board is added to the magnets' stand from below to prevent hot vapor from heating up the magnets. Subsequently, the loop is immersed in the hot fluid, and the valves of the cooling cylinder are opened while the temperatures of the hot bath and the cold bath are monitored on the display of the cooling circulator and of the Ultraterm heating unit. Liquid thermometers immersed in the baths confirmed these readings. The cold bath temperature was maintained at 0°C with a flow of 14 l/min, and this temperature was attained by the addition of an antifreeze solution to the circulating fluid. The increase in temperature in the hot bath is of the order of 5°C per reading, starting at 25°C and ending at 80°C. When the temperature stabilized at the required value, 5 min are given to the system to reach steady-state conditions, then wires emanating from the electrodes are short circuited to cancel any static charge build up, and reading of the steady-state voltage is taken. The steady tests on any one module are repeated at least twice, and readings are compared. The uncertainty in the recorded electrodes' output voltage, and the driving difference $\Delta T$ were well within the precision limits of the voltage and temperature measuring devices given earlier.

The computerized data acquisition system is used for module 4 due to the large number of simultaneous readings to be taken in the experiment. For this purpose a code is written to do the sampling. The readings of the system are streamed to a spreadsheet, where the calculations are made for averaging the readings. A special blue ink die, a chronometer, and a digital camera are used to measure bulk velocity and visualize the flow for the case when no magnetic field is present because the magnets blocked the flow view when deployed. An error of up to 6% is incurred in the measured bulk flow velocity as the dye moves along the loop down from one side and up to the other side.

## Analytical One-Dimensional Model

#### Flow and Heat Transfer Equations

The one-dimensional model for the loop is based on the solution of Ghaddar[8] for a plane channel closed loop placed in a transverse magnetic field. In this work, the solution will be modified to represent a flow in a cylindrical channel of diameter $D$. The transverse magnetic field $B_0$ is applied perpendicular to gravity only in the middle insulated portion of the loop of height $2l$ and not to the full height of the loop, as shown in Fig. 1. The Boussinesq fluid contained in the loop is electrically conducting with an electrical conductivity $\sigma$ and a coefficient of thermal expansion $\beta$. The magnetic field $B_0$ is applied perpendicular to gravity in the $x$ direction. The thermophysical properties of the fluid at a reference temperature $T_0$ are assumed to be constant except for the density $\rho$, which is related to temperature according to $\rho = \rho_0[1 - \beta(T - T_0)]$. The lower portion of the loop wall is isothermally heated to $T_H$, while the upper part is isothermally cooled to the reference temperature $T_C$. To simplify the coordinate system, circular ends at the top and bottom parts of the loop are considered to be straight, and the origin of the $y$ axis is placed at the midpoint of the left segment of the loop, parallel to the flow direction as it moves against gravity from 0 to $2L$ and then with gravity from $-2L$ to 0. Axial heat conduction and

viscous heating are neglected, and the steady conservation equations are written in terms of the cross sectionally averaged velocity $V_0$ and bulk temperature $T_b$ as follows.

Continuity:

$$V_0 = \text{const} \tag{1}$$

Momentum:

$$0 = -\frac{\partial p}{\partial y} - \rho g - \sigma V_0 B_0^2 - \frac{4\tau_s}{D} \tag{2}$$

Energy in the isothermal regions, $-2L + l \le y \le -l$ and $l \le y \le 2L - l$:

$$\rho C\left[V_0 \frac{\partial T_b}{\partial y}\right] = \frac{4h}{D}\{T_w - T_b(y)\} + \sigma V_0^2 B_0^2 \tag{3a}$$

Energy in the insulated regions, $-l \le y \le +l$ and $2L - l \le y \ge -2L + l$:

$$\rho C\left[V_0 \frac{\partial T_b}{\partial y}\right] = 0 \tag{3b}$$

where $T_w$ is the loop wall temperature in the isothermal regions defined by

$$T_w = T_H \tag{4a}$$

for $-2L + l \le y \le -l$ and

$$T_w = T_C \tag{4b}$$

for $l \le y \le 2L - l$. Equations (1–3) are solved for steady state conditions. Following the solution of Ghaddar,[8] the energy equations (3a) and (3b) are solved first for the temperature in dimensionless form, $\theta_b = (T_b - T_C)/(T_H - T_C)$, along the full loop as

$$\theta_b = \begin{cases} 1 + Ae^{-my/d}, & -2L + l \le y \le -l \\ Be^{-my/d}, & +l \le y \le 2L - l \end{cases} \tag{5a}$$

where $A$ and $B$ are the dimensionless terms defined as

$$A = \frac{\{1 - \exp[-2m(L - l)/d]\}}{\{\exp[-m(2L - 3l)/d] - \exp[m(2L - l)/d]\}} \tag{5b}$$

$$B = A\exp(2ml/d) + \exp(m\ell/d) \tag{5c}$$

where $m$ is the Stanton number ($m = Nu/RePr$), $Nu$ is the Nusselt number of the flow, and $Pr$ is the Prandtl number of the fluid. The momentum equation (2), which shows a balance between buoyancy, Lorentz forces, and friction forces, is integrated along the loop. The pressure variation in the loop is due to gravity, which is the driving force for the whole motion. The shear stress force can be expressed in terms of the friction factor as $\tau_s = f\rho_0 V_0^2/2$, where the friction factor is $f = 16/Re_D$ for laminar pipe flow. The Lorentz force in the present solution is integrated over the length of the insulated region $4l$, whereas the friction force will be integrated over the full length of the loop $4L$. Then, for the present setup, the predicted analytical relation between the induced velocity and the imposed temperature difference is given in terms of dimensionless parameters as

$$Gr = \frac{[128Re^2 f + 4ReHa^2(l/L)]}{2(l/L)(S) + m(K)/(L/d)} \tag{6a}$$

where $K$ and $S$ are

$$K = \tfrac{1}{2}\left[A\left(2e^{mL} - e^{ml} - e^{m(2L-l)}\right) + B\left(e^{-ml} + e^{-m(2L-l)} - 2e^{-mL}\right)\right] \tag{6b}$$

$$S = \tfrac{1}{2}\left[A\left(e^{ml} - e^{m(2L-l)}\right) + B\left(e^{-ml} - e^{-m(2L-l)}\right)\right] \tag{6c}$$

$\Delta T = T_H - T_C$ is the temperature difference between hot and the cold walls. Note that in the solution there is no restriction on the relative size, $l/L$, of the insulated region to the isothermal regions. In the high Hartmann number limit ($Ha > 100$), the friction factor $f$ is significantly higher than the simple value used in the present model where the ratio $f_{(Ha=0)}/f_{(Ha>100)} \sim (Ha)^{-1}$ according to Grandet et al.[11] The Hartmann number range for the presented solution is then limited to $Ha < 20$, where the magnetic field effect on the shear stress compared to $Ha = 0$ case can be neglected.

**Electric Field and Current Equations**

For electrolytes, the design of the electrodes and their electric connections affect significantly the electric output predicted from the system. Electric output equations are derived for the three combinations of electrode types and electric connections as described in the experimental setup section.

*Case 1: Continuous Electrodes Faraday Generator Connection*

The external open-circuit electric field $E_{oc}$ (volts per meter), open-circuit voltage $V_{oc}$ (volts), and load electric fields $E_0$ (volts per meter) are given by

$$E_{oc} = V_0 B_0 \tag{7a}$$

$$V_{oc} = E_{oc} \cdot D_e \tag{7b}$$

$$E_0 = K V_0 B_0 \tag{7c}$$

where $K$ is the load factor defined as $K = E_0/E_{oc}$. The induced electric field (volts per meter) across the fluid is

$$E_{ind} = V_0 B_0 (K - 1) \tag{8}$$

The load current density (amphere per square meter) perpendicular to the flow direction is

$$J_x = \{\sigma/[1 + (\omega\tau)^2]\} V_0 B_0 (K - 1) \tag{9}$$

The total current ampere is

$$I = J_x \times A_{\text{electrode}} \tag{10}$$

where $A_{\text{electrode}}$ is the area of the electrodes and $\omega\tau$ is the Hall parameter. For liquids, in an appropriately designed apparatus, potential differences related to the Hall effect may be measured in principle and $\omega\tau$ can be obtained.

The generated electrical power (watts per cubic meter) per unit volume of fluid enclosed between electrodes of the Faraday generator is $J_x E_0$ given by

$$P = \{\sigma/[1 + (\omega\tau)^2]\} V_0^2 B_0^2 K(K - 1) \tag{11}$$

which shows the resulting drop in the performance of the Faraday generator due to the Hall effect. The generated power for $K < 1$ is negative, whereas the mechanical push power or input is positive by definition.

*Case 2: Segmented Electrode Faraday Generator*[1]

The output of a Faraday generator with continuous electrodes will be seriously reduced due to the Hall current closing through

the electrodes. To avoid this and to break the return path of the Hall current, segmented electrodes are usually used such that each pair of electrodes has its own individual load. To minimize the Hall current, the electrodes have to be very narrow in the $y$ direction relative to the width of the channel. With segmented electrodes, the Faraday current (amphere per square meter) and power output (watt per cubic meter) of Eqs. (9) and (11) output will be replaced by

$$J_x = \sigma V_0 B_0 (K - 1) \tag{12}$$

$$P = -\sigma V_0^2 B_0^2 K (1 - K) \tag{13}$$

*Case 3: Segmented-Electrodes Hall Generator Connection*[1]

When $\omega\tau$ becomes very large, the Hall voltage becomes large compared with the Faraday voltage. The Faraday current $J_y$ is made as large as possible by short circuiting the electrode pairs. This leads to a maximum current along the axis and is extracted by connecting a single load to the first and the last pairs. The open-circuit axial electric field is:

$$E_{oc} = -\omega\tau V_0 B_0 \tag{14}$$

The load factor for the Hall generator becomes

$$K = -(E_{oy}/\omega\tau V_0 B_0) \tag{15}$$

Experimental studies of the Hall effect for electrolytes report potential differences up to several tens of millivolts in constant imposed electric fields. The Hall parameter for liquids is directly proportional to the imposed magnetic field strength.[2] Although the ionic Hall parameter values computed from different theories agree, this does not mean that the effect of the magnetic field on electrolyte conductivity is clearly known. The development of a relatively simple theory explaining all experimental findings remains a serious challenge to theoretical electrochemists.[2] The Hall effect can substantially decrease $J_x$, and the short-circuited Hall current flux (amphere per meter squared) in the flow direction $y$ is

$$J_y = \{\sigma/[1 + (\omega\tau)^2]\}\omega\tau V_0 B_0 (K - 1) \tag{16}$$

The Hall current can exceed the Faraday current flux if $\omega\tau > 1$.

It is clear that the open-circuit electric field and voltage for the Hall connected system is larger than the segmented Faraday system by a factor of $\omega\tau$, whereas the short-circuit current is smaller by the factor $\omega\tau/[1 + (\omega\tau)^2]$. The power output (watt per cubic meter) of the Hall connected system is

$$P_H = -J_{oy} E_{oy} = \{(\omega\tau)^2/[1 + (\omega\tau)^2]\} V_0^2 B_0^2 \sigma K_h (K_h - 1) \tag{17}$$

## Results and Discussion

### Flow Hydrodynamics

Visualizations of the steady flow around the thermosyphonic loop in the transparent and insulated connecting region (module 3 with $L/D = 8.74$, $l/D = 2.67$, and $D = 24.3$ mm) are shown for $\Delta T = 80 \pm 0.2$°C in Fig. 3, where Figs. 3a and 3b are for the downgoing flow side and Figs. 3c and 3d are for the upgoing flow side of the same loop. The fluid moving downward in the visualized zero-flux region is at its coldest state in the loop after circulating through the top heat sink and has a flat almost parabolic velocity profile, where the flow core has a higher velocity than the wall layer. The fluid moving upward in the visualized zero-flux region (Figs. 3c and 3d) is at its hottest state in the loop after circulating through the bottom heat source. The velocity profile of the upward moving fluid clearly shows the buoyancy-driven hotter wall jets that mobilize the bulk of the flow upward. The fluid wall layer in this case has a higher velocity than the central core velocity.

Experimentally measured velocity is compared with the analytically predicted velocity at $Ha = 0$, using Eq. (6). In the one-dimensional model, the flow Nusselt number is assumed constant throughout the loop. This assumption is valid for small values of $V_0$. For moderate values of $V_0$, the heat transfer is generally improved

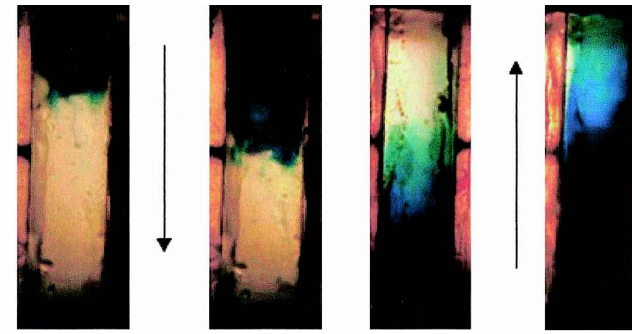


**Fig. 3 Flow visualization at $\Delta T = 80 \pm 0.2$°C: a) downflow at $t = 2$s, b) downflow at $t = 3$s, c) upflow at $t = 15$s, and d) upflow at $t = 16$s.**

with $h$ varying as $h\alpha V_0^{1/3}$ in the laminar flow regime.[4] Figures 4a–4d show the variation of analytically predicted and experimentally calculated Reynolds number with Grashof number at different values of Nusselt for the different prototypes. The liquid properties are evaluated at the mean temperature of the fluid, $(T_H + T_C)/2$. A correlation for a Nusselt number as a function of Reynolds ($Nu = 2.304Re^{1/3} + C_1$), is developed to best fit the data for the loop prototypes, where the coefficient $C_1$ depends on $L/D$ ratio of the loop modules. [$C_1 = -9.5$, $-10.0$, $-11.5$ and $-12$ for $L/D = 11$ (module 1), $L/D = 10$ (module 3), $L/D = 8.74$ (module 4), and $L/D = 8.5$ (module 2), respectively.] When the correlation gives $Nu$ smaller than isothermal laminar pipe convection of 3.66, the value of Nusselt number of 3.66 overrides. When the correlation is substituted directly into the analytical one-dimensional model, the predicted values of the Reynolds number agree well with experimental data, as shown in Fig. 5, where the error between the analytical model and the experimental Reynolds number at varying Grashof number is reduced to less than 5%. Although the analytical one-dimensional model has limitations due to neglecting the loop bends at the upper and lower parts and other assumptions with regard to constant properties, it does give good predictions of the induced velocity of the flow.

### Analytical Model Predictions of ReHa

The product of the Reynolds and Hartmann numbers is a dimensionless parameter proportional to the open-circuit voltage for the continuous electrodes Faraday generator, $ReHa = E_{oc} D^2 [(\sigma/\mu)^{1/2}]/\nu$. The open-circuit voltage parameter $E_{oc} D^2 [(\sigma/\mu)^{1/2}]/\nu$ in the developed analytical model is not explicitly expressed in a closed form in terms of the other parameters of the system but is calculated from the implicit numerical solution of Eqs. (5) and (6) as a function of Hartmann number and Grashof number, using the experimental correlation of Nusselt number. Figure 6 shows the product $ReHa$ as a function of Hartmann number $Ha$ at fixed Grashof number. (The one-dimensional model is applicable for the present experimental conditions.) It is clear that there is an optimal Hartmann number $Ha$ for maximum induced voltage. The optimal Hartmann number increases as the Grashof number is increased. ($Ha_{opt} = 12.5$ and 14.5 for $Gr = 3 \times 10^6$ and $Gr = 5 \times 10^7$, respectively.) The maximum Hartmann number imposed in the experimental work is about 1.2, which is one order of magnitude less than the analytically predicted values for maximum induced open-circuit voltage.

### Electrical Characteristics of Thermosyphonic MHD Flow of the Hall Generator

Experimental tests are made on module 1 Hall generator connection to investigate the effect of using different salts on the open-circuit voltage. Sample of results are shown in Fig. 7 for experiments conducted with a magnetic field of $0.1 \pm 10^{-4}$ $T$ and a conductivity of $20 \pm 0.1$ S/m, and the used salts were MgCl 6–hydrates, NaCl, and KCl, respectively.

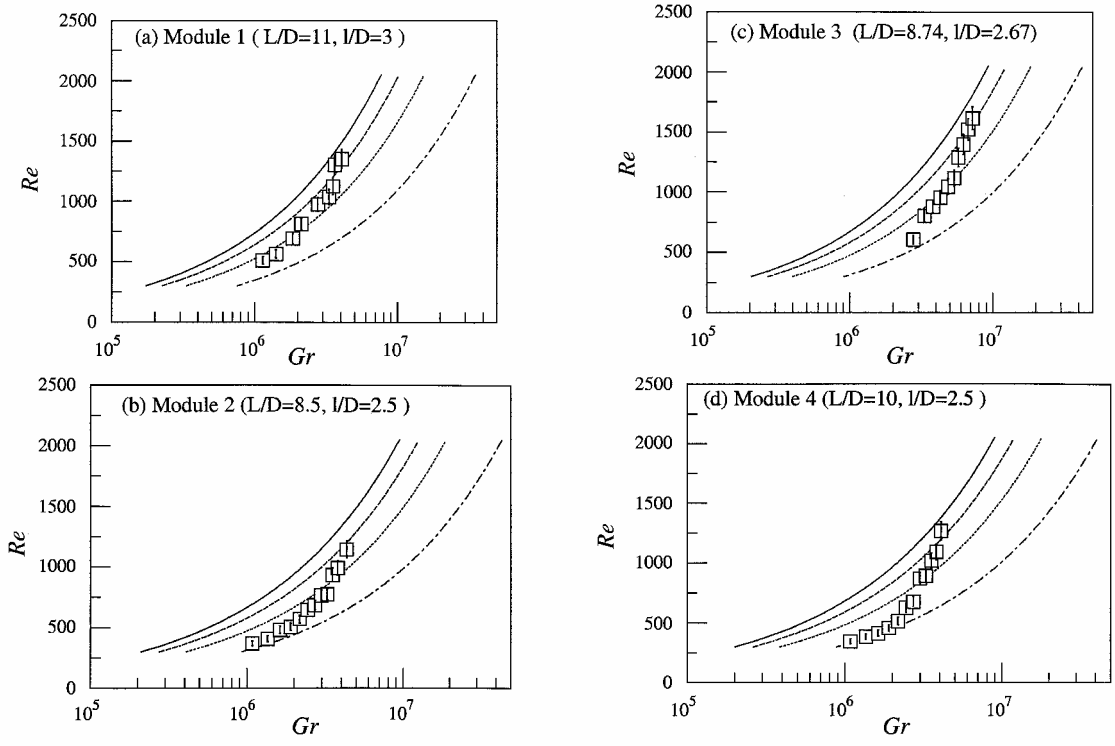


**Fig. 4 Variation of analytically predicted and experimentally calculated Reynolds with Grashof number at different values of Nusselt number for the different loop prototypes.**

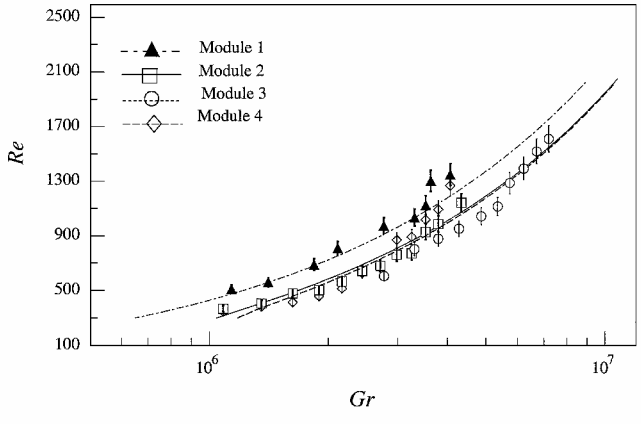


**Fig. 5 Experimental data vs analytical model using the Nusselt number correlation to Reynolds in the analytical one-dimensional model.**

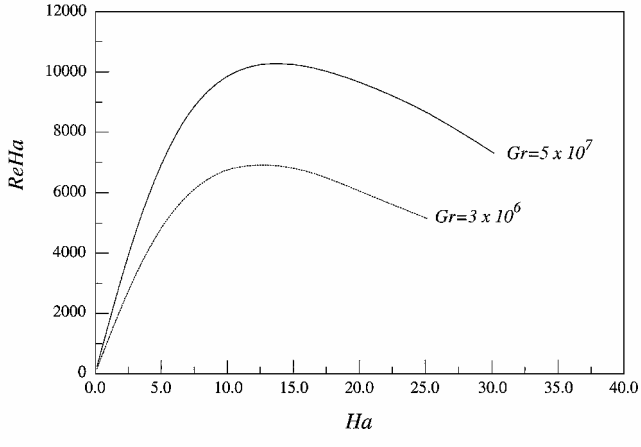


**Fig. 6 Product *ReHa* as a function of Hartmann number *Ha* at fixed Grashof number as predicted by the analytical one-dimensional model.**

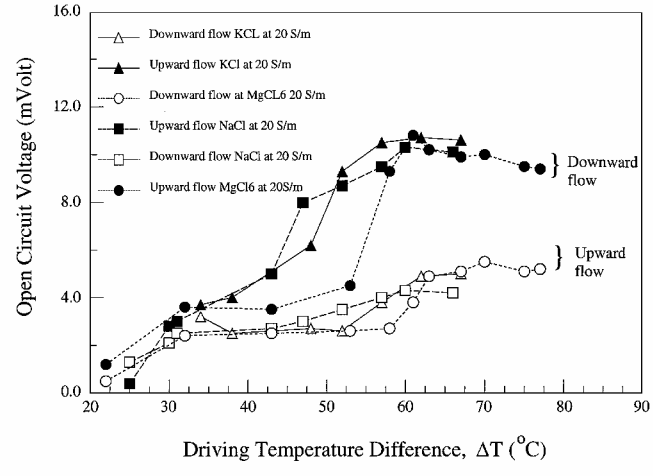


**Fig. 7 Open-circuit voltage output (millivolts) (measurement error ±0.001 mV) of segmented Hall generator (module 1) vs $\Delta T$ (probable measurement error ±0.2°C) at 20 ± 0.1 S/m and 0.1 ± 0.0001 T.**

The upward flow induces higher voltage output than the downward flow. This is mainly due to the higher velocity in the upward flow. The accelerating upward flow is warmer than the downgoing flow, and hence, it has a lower bulk density than the downward flow. To satisfy mass conservation in the constant diameter loop, the lower density upward flow will have a higher velocity than the higher density downward flow. This is not the only effect because the velocity profiles across the hot domain are not parabolic because the flow is driven by natural convection, having higher velocity near the wall and less at the center. Also the magnetic field is low at the center and higher at the walls, and so this region of high magnetic field and high velocity near the wall of the upflow contributes in the higher voltage in that region. The upflow voltage increases smoothly from 2 ± 0.001 to 11 ± 0.001 mV, and the downward flow voltage increases from 1 ± 0.001 to 5 ± 0.001 mV. The cooler side shows less discrepancy in the measure of voltage between the different solutions than the hotter side, and this may be attributed to the fact that

the accelerating side of the loop has a hotter fluid near the wall, that is, near the electrode surface, and is more susceptible to having flow transition and mixing than the cold downward flow. The electrical conductivity is highly dependent on temperature, leading to a high Hall effect. For different solutions, this effect causes local deviations in the wall layer temperature in the vicinity of the electrodes and in the measured voltage between them, even though the bulk electrical conductivity at 20°C is the same for all of the solutions.

*Hall Parameter $\omega\tau$ Determination*

The Hall parameter is not documented in the literature for electrolytes due to the lack of interest in using it as a working fluid in generators. However, a revived interest in MHD of electrolytic fluids has been emerging.[1,2,12] It is known that the Hall parameter $\omega\tau$ is dependent on the magnetic field strength, temperature, and electric conductivity of the fluid. From Eq. (14), the Hall parameter can be evaluated at any driving $\Delta T$ of the thermosyphon from the measured voltage outputs at both sides of the loop for the segmented electrode Hall generator connection and the measured values of velocity and magnetic field strength. The correlating parameter for $\omega\tau$ is the bulk flow temperature of the working fluid inside the loop and not the driving temperature difference. The bulk flow absolute temperatures in the insulated regions of the loop (upward hot-flow side and downward cold-flow side) are calculated from the analytical temperature distribution derived in Eq. (5) using the measured $\Delta T$. Figure 8 shows the estimated Hall parameter as a function of the absolute bulk temperature of the fluid as determined from the experiments and the present one-dimensional analytical model at $B_0 = 0.1 \pm 0.0001$ T and at nominal $\sigma$ values at 20°C of $15 \pm 0.1$ S/m and $20 \pm 0.1$ S/m, corresponding to $Ha = 0.3$ and 0.35, respectively. The probable error in the estimated Hall parameter is ±5.5% and is directly shown in Fig. 8, taking into consideration the precision error in $V_0$(±6%), in $B_0$ (±2%), and measured voltage output (±0.1%). The estimated error in the absolute bulk temperature calculations is directly related to the measured velocity used in finding the analytical temperature distribution. An error of 5% in the velocity would introduce an error of 0.4% in the value of $\theta_b$ with a maximum error of ±0.32°C when $\Delta T = 80$°C. A linear correlation of $\omega\tau$ vs temperature for the laminar MHD electrolyte flow that yields the best fit is given by

$$(\omega\tau)_{Ha=0.35} = 4.4668T_{\text{abs}} - 1243.85 \tag{18a}$$

$$(\omega\tau)_{Ha=0.3} = 1.3707T_{\text{abs}} - 375.027 \tag{18b}$$

Equations (18a) and (18b) have correlation parameters of 0.968 and 0.975, respectively.

Thus, for this Hall generator, the open-circuit voltage is larger by a factor of $\omega\tau$ than the expected Faraday generator value, and hence, the short-circuit current is smaller by a factor of $\omega\tau/[1+(\omega\tau)^2]$. For $\omega\tau \gg 1$, the factor decreasing the short-circuit current approaches $1/\omega\tau$, and the output power will be affected seriously.

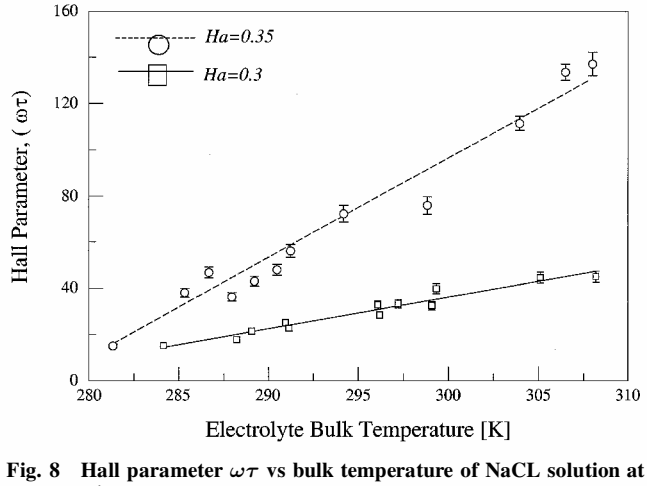


**Fig. 8 Hall parameter $\omega\tau$ vs bulk temperature of NaCL solution at $B_0 = 0.1 \pm 0.0001$ T.**

**Theoretically Modified Open-Circuit Voltage Output for the Hall Generator**

The values of the dimensionless open-circuit voltage determined experimentally (from the measured magnetic field and velocity) and predicted analytically using Ghaddar's model[8] are plotted against the value of the Grashof number and then the analytical values of *ReHa* are multiplied by the experimentally determined Hall parameter value for the given temperature difference. Figure 9 shows the experimental results of the dimensionless measured open-circuit voltages and the analytical one-dimensional model predictions of open circuit voltage for a segmented Hall generator connection in dimensionless form for both $(\omega\tau)(ReHa)$ and *ReHa*. The error in comparing the analytical to the experimental dimensionless open-circuit output was 8.7%. The modified analytical model has captured all of the physical features of the flow and its electric output. It represents also a second check of the accuracy of the calculations of the Hall parameter factor.

**Electric Output of Faraday Generator**

The loss of power due to the Hall effect in a continuous electrode Faraday generator is investigated. Modules 2 and 3 are continuous electrode Faraday generators. Experiments were conducted at two nominal conductivities of $15 \pm 0.1$ and $20 \pm 0.1$ S/m and various magnetic field levels from $0.1 \pm 0.0001$ to $0.225 \pm 0.0001$ T. Figures 10a and 10b show the measured open circuit vs the driving

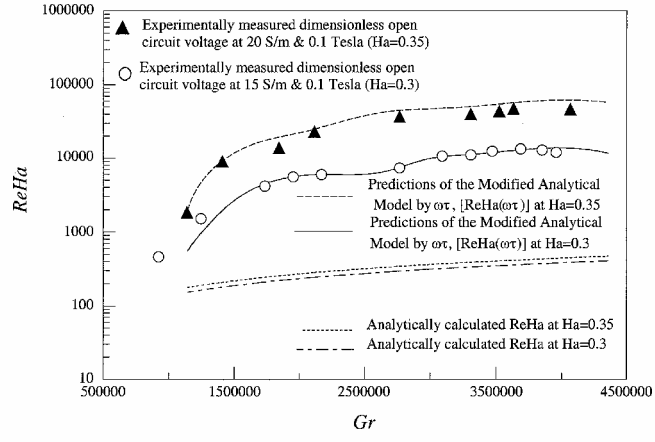


**Fig. 9 Dimensionless measured open circuit voltages and the predictions of the analytical one-dimensional model of *ReHa* and $ReHa^*(\omega\tau)$ for the segmented Hall generator connection of module 1.**

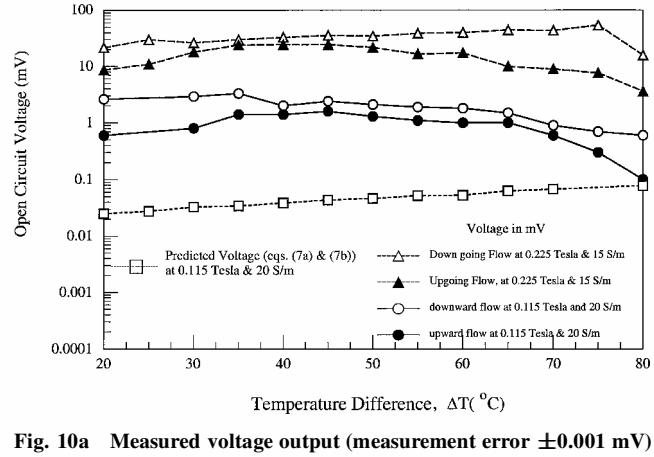


**Fig. 10a Measured voltage output (measurement error ±0.001 mV) vs driving temperature difference $\Delta T$ (probable measurement error ±0.2°C) for round continuous electrodes of module 2, at $15 \pm 0.1$ S/m, $0.225 \pm 0.0001$ T, and at $20 \pm 0.1$ S/m, $0.115 \pm 0.0001$ T.**

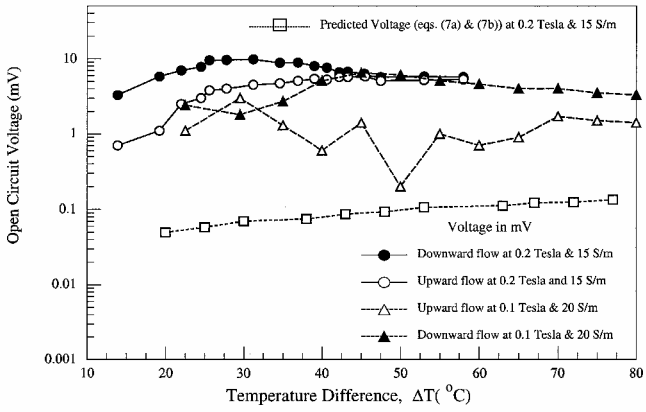


**Fig. 10b Measured voltage output (millivolts) (measurement error ±0.001 mV) vs driving temperature difference $\Delta T$ (probable measurement error ±0.2°C) for parallel square continuous electrodes of module 3 at 15 ± 0.1 S/m, 0.2 ± 0.0001 T, and at 20 ± 0.1 S/m, 0.1 ± 0.0001 T.**

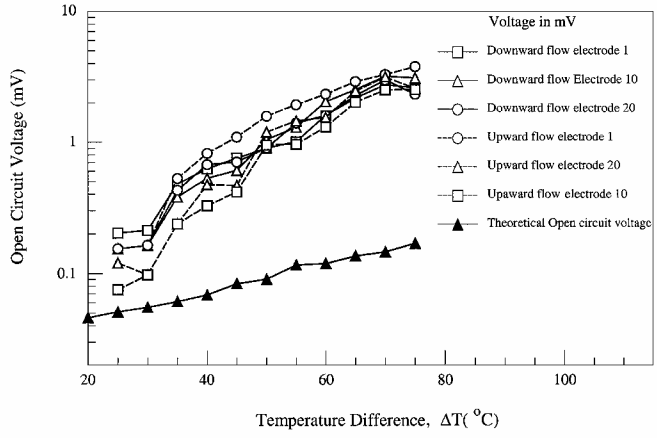


**Fig. 11 Theoretical and experimental voltage output (millivolts) (measurement error ±0.001 mV) vs driving temperature difference $\Delta T$ (probable measurement error ±0.2°C) for the segmented electrodes and Faraday-type connection of module 4 at 20 ± 0.1 S/m, 0.225 ± 0.0001 T.**

temperature difference between the heat source and heat sink for 1) the round continuous electrodes of module 2 at 15 ± 0.1 S/m, 0.225 ± 0.001 T, and at 20 ± 0.1 S/m, 0.115 ± 0.0001 T, and 2) the parallel square continuous electrodes of module 3 at 15 ± 0.1 S/m, 0.2 ± 0.0001 T, and at 20 ± 0.1 S/m, 0.1 ± 0.0001 T. Also in Figs. 10a and 10b, the expected open-circuit voltage is shown as calculated using Eqs. (7a) and (7b) from measured average bulk velocity and imposed magnetic field strength at 20 ± 0.1 S/m and 0.115 ± 0.0001 T of the round module 2 and at 15 ± 0.1 S/m and 0.2 ± 0.0001 T of module 3, respectively.

The continuous electrodes Faraday generator experiments resulted in higher voltage output for downward flow than the upward flow output, unlike the Hall generator segmented electrodes output, which showed higher voltage output for the upward hot-bulk flow side. Furthermore, for all of the experiments of modules 2 and 3, the open-circuit voltage output of the downward flow increases with temperature difference till the value of $\Delta T$ reaches 40 ± 0.2°C or higher, then the downward flow output voltage drops until both upward and downward flow voltages are the same. This phenomenon of surge in output of the downflow voltage curve is attributed to both flow transition to turbulence and the Hall effect. In modules 2 and 3, the measured open-circuit voltage is about two orders of magnitude higher than what is expected from theory due to the Hall effect that is based on the $\omega\tau$ parameter and on the internal resistances that are inversely proportional to the conductivity.[1] The conductivity of an electrolyte varies with temperature. As the temperature rises, molecular movement, including that of ions in the solution, increases dramatically. This causes an increase in conductivity. The amount of change in conductivity per degree Celsius is referred to as the temperature coefficient. The temperature coefficient of an electrolyte is expressed in percent divided by degree Celsius (%/°C) at a particular temperature. The temperature coefficient of NaCl, with respect to the reference temperature at 25°C, at 15 S/m is 2.12%/°C and at 20 S/m is 2.16%/°C (Ref. 12). On the other hand, as the temperature increases, the conductivity increases, and the Hall voltage decreases. The Hall effect is larger in the downward flow of the loop, where the temperature near the wall is lower than the center, leading to a substantial drop in the conductivity and, thus, an increase in the Hall voltage.

As the driving temperature $\Delta T$ increases, the output voltage of the downward flow decreases due to the transition to turbulent flow that induces better mixing, flatter velocity profile, and minimal bulk temperature difference between the two sides of the loop. This reduces the Hall effect in the downward flow and brings both upward and downward flow to induce the same voltage. According to Creveling et al.,[5] the turbulent region in thermosyphonic loops starts at $1000 < Re < 1500$, but in the present case, due to the vibration created by the circulation pump of the heating bath, this turbulent region can start at lower Reynolds numbers. This transition from laminar to turbulent flow promotes mixing of the fluid, and therefore, the cold temperature layer at the wall is broken, and a more even distribution of the electrical conductivity exists in the flow reducing the Hall effect.

### Controlling the Hall Effect with a Segmented Electrode Faraday Generator Type

Reducing the electrode area by segmenting the electrodes to 2 mm strips that are 2 mm apart as in module 4 will break down the Hall effect. In this module, the segmentation ratio (electrode strips spacing/$D_e$) is equal to 0.2, which still causes a significant loss in power,[9] but not as significant as the segmentation ratios of 3.2 and 5.45 for modules 2 and 3, respectively.

Figure 11 shows the measured open-circuit output of the segmented electrode–Faraday generator of three representative readings from electrode strips 1, 10, and 20 on each side of the loop at a magnetic field of 0.225 ± 0.0001 T and a conductivity of 20 ± 0.1 S/m. In Fig. 11, the ideal theoretical open-circuit voltage is also shown at 0.225 ± 0.0001 T.

We are still away from the theoretical output voltage of the generator because of the Hall effect that reduces the power output of the loop. However, the output voltage is closer to the theoretical output, where it is only one order of magnitude higher from the ideal output of the generator. This is an improvement over the continuous electrodes Hall effect where the open-circuit voltage output is larger by a factor of 100 from the ideal expected output.

## Conclusions

An experimental and analytical study is presented of thermosyphonic MHD flow of electrolyte solutions. A thermosyphonic closed-loop MHD flow system is built and tested as a Hall generator, a continuous electrodes Faraday generator, and a segmented electrodes Faraday generator. The work findings are summarized as follows:

1) The analytical one-dimensional model compared favourably with the experimental results when modified to account for the Hall parameter.

2) The output voltage increases with increasing temperature difference.

3) The Hall parameter was correlated to the electrolyte solution temperature at fixed magnetic field strength. The dependence on temperature disturbed the power output from the electrodes. Determination of the Hall parameter for electrolytes is important in applications where the longitudinal Hall current gives a transverse body force, which in turn leads to induced transverse gradients in pressure and velocity. This effect is important in studies of boundary-layer control by electric and magnetic fields in submarine propulsion in weakly conducting fluids such as seawater.

4) The type of the salt did not significantly influence the output voltage as much as the solution electrical conductivity. The MHD

flow generated much higher voltages than expected on the expense of the current yielding low-power output. This was mainly because electrolyte solutions have high Hall parameter $\omega\tau$ values that are highly dependent on temperature and electrical conductivity. Both the temperature and the conductivity were constantly changing in the thermosyphon flow, which disturbed the power output, by creating overshoots and significant drops in the value of the electrical conductivity in the wall layer and, hence, increasing the Hall voltage.

## Acknowledgments

The authors acknowledge the financial support of the Lebanese National Council for Scientific Research under Grant 323040 and the American University of Beirut Research Board under Grant 17996073615. The help of Farid Chaaban on the sizing of the permanent magnets is greatly acknowledged.

## References

[1]Messerle, H. K., *Magnetohydrodynamic Electrical Power Generation*, Wiley, New York, 1995, pp. 127–133.

[2]Fahidy, T. Z., "Magnetoelectrolysis," *Journal of Applied Electrochemistry*, No. 13, 1993, pp. 553–563.

[3]Weier, T., Fey, U., and Gerberth, G., "Boundary Layer Control by Means of Electromagnetic Forces," *European Community on Flow, Turbulence and Combustion Bulletin*, Vol. 44, 2000, pp. 36–40.

[4]Weier, T., Gerberth, G., Mustschke, G., and Platacis, E., "Experiments on Cylinder Wake Stabilization in an Electrolyte Solution by Means of Electromagnetic Forces," *Experimental Thermal and Fluid Sciences*, Vol. 16, 1998, pp. 84–91.

[5]Creveling, H. F., De Paz, J. F., Baladi, J. Y., and Schoenhals, R. J., "Stability Characteristics of a Single-Phase Free Convection Loop," *Journal of Fluid Mechanics*, Vol. 67, Pt. 1, 1979, pp. 65–84.

[6]Ehrhard, P., Karcher, C., and Muller, U., "Dynamical Behaviour of Natural Convection in a Double Loop System," *Experimental Heat Transfer*, Vol. 2, 1989, pp. 13–26.

[7]Ehrhard, P., and Muelleur, S., "Dynamical Behaviour of Natural Convection in a Single Phase Loop," *Journal of Fluid Mechanics*, Vol. 217, 1990, pp. 487–509.

[8]Ghaddar, N., "Analytical Model of Induced Electric Current from a Free-Convection Loop Placed in a Transverse Magnetic Field," *International Journal of Heat and Mass Transfer*, Vol. 41, No. 8–9, 1998, pp. 1075–1086.

[9]Ghaddar, N., "Numerical Simulation of a Vertical Thermosyphonic Loop placed in a Transverse Magnetic Field," *Numerical Heat Transfer*, Vol. 32, No. 2, 1997, pp. 231–246.

[10]Parker, R. J., *Advances in Permanent Magnetism*, Wiley, New York, 1990, pp. 62–71.

[11]Grandet, J. P., Alboussieri, T., and Moureau, T., "Buoyancy Driven Convection in a Rectangular Enclosure with a Transverse Magnetic Field," *International Journal of Heat and Mass Transfer*, Vol. 35, No. 4, 1992, pp. 741–748.

[12]Henoch, C., and Stace, J., "Experimental Investigation of a Salt Water Turbulent Boundary Layer Modified by an Applied Streamwise Magnetohydrodynamic Body Force," *Physics of Fluids*, Vol. 7, 1995, pp. 1371–1383.